AUTHOR QUERY FORM

AIP American Institute of Physics	**Journal: J. Chem. Phys.** **Article Number: 011248JCP**	**Please provide your responses and any corrections by annotating this PDF and uploading it to AIP's eProof website as detailed in the Welcome email.**

Dear Author,

Below are the queries associated with your article. Please answer all of these queries before sending the proof back to AIP.

Location in article	**Query / Remark: click on the Q link to navigate to the appropriate spot in the proof. There, insert your comments as a PDF annotation.**
Q1	AU: Please verify the author names in Ref. 12.

Thank you for your assistance.

Hollow core photonic crystal fiber based viscometer with Raman spectroscopy

L. E. Horan,[1,2,a)] A. A. Ruth,[2,b)] and F. C. Garcia Gunning[1,2,c)]
[1]*Tyndall National Institute, University College Cork, Lee Maltings, Cork, Ireland*
[2]*Department of Physics, University College Cork, Lee Maltings, Cork, Ireland*

(Received 27 September 2012; accepted 28 November 2012; published online XX XX XXXX)

The velocity of a liquid flowing through the core of a hollow core photonic crystal fiber (driven by capillary forces) is used for the determination of a liquid's viscosity, using volumes of less than 10 nl. The simple optical technique used is based on the change in propagation characteristics of the fiber as it fills with the liquid of interest via capillary action, monitored by a laser source. Furthermore, the liquid filled hollow core photonic crystal fiber is then used as a vessel to collect Raman scattering from the sample to determine the molecular fingerprint of the liquid under study. This approach has a wide variety of indicative uses in cases where nano-liter samples are necessary. We use 10–12 cm lengths of hollow core photonic crystal fibers to determine the viscosity and Raman spectra of small volumes of two types of monosaccharides diluted in a phosphate buffer solution to demonstrate the principle. The observed Raman signal is strongest when only the core of the hollow core photonic crystal fiber is filled, and gradually decays as the rest of the fiber fills with the sample. © *2012 American Institute of Physics*. [http://dx.doi.org/10.1063/1.4771659]

I. INTRODUCTION

Hollow core photonic crystal fibers (HC-PCFs)[1–3] have attracted a lot of interest due to the possibility of inserting liquids into the capillaries for optical sensing in biological[4,5] and chemical applications.[6] These applications tend to exploit its main optical property called the photonic bandgap (PBG) effect,[7,8] where light guidance occurs within the hollow core only for certain wavelengths. Another interesting effect in such fibers, also used in sensing, is the bandgap shift that occurs when all capillaries are filled with a liquid sample.[9] In this case, light propagation occurs at significantly shorter wavelengths than the original PBG. The shift in PBG can be estimated utilizing scalar wave equations.[8] Finally, if only the core of the fiber is selectively filled, the optical propagation once again changes, with the physical mechanism changing from PBG to index-like guidance.[10] In this paper, we exploit all these changes in propagation properties during the insertion of a liquid into the fiber in order to determine its dynamic viscosity by its flow through the hollow capillaries. The flow of liquids through ordinary capillaries has been extensively studied and is widely used to determine viscosities.[11] Compared with current commercially available capillary viscometers (1–10 ml volume samples required), the proposed technique here requires only nanoliter quantities of liquid for any measurement.

The technique shown here was tested using phosphate buffer saline (PBS) solutions of the monosaccharides glucose and fructose across a range of concentrations. Monosaccharides are ubiquitous in life and food sciences,[12] e.g., as a source of energy in living organisms and as a fundamental ingredient in food for the enhancement of flavour or as a preservative. Knowing the viscosity of saccharide solutions, for example, is important for the measurement of the degree of sweetness.[13] Here we will also show that, with a slight modification, it is possible to characterize the composition of the liquid sample via the detection of vibrational Raman scattering within the hollow core. HC-PCF has been shown to be an excellent medium for the collection of Raman scatter[14,15] when it is filled with solutions for two reasons: (a) the resultant wavelength shift with a broad PBG window enables the guiding of both the excitation light and the Raman scatter at visible wavelengths through the fiber directly to the detector, leading to high collection efficiencies; and (b) the possibility of filling long lengths of fibers enhances the light-liquid interaction path length and increases the measurement sensitivity. Therefore, this viscometer system can provide information about the molecular identity of the solution in question without extensive further analysis.

II. NANOLITER VISCOMETER

A. Principle

In this paper, we use a simple force model derived from Nielsen *et al.*,[16] which is based on the Lucas-Washburn equation.[17] The Lucas-Washburn equation describes the time it takes for a liquid to flow through a capillary. This allows us to determine the time it takes to fill a certain length of HC-PCF, and thus the average velocity of the liquid flow. This model takes into account all forces that affect capillary flow: the capillary and overpressure forces, which are balanced by frictional and gravitational forces. In our experiments, overpressure was not applied and gravity can be neglected due to the small core radius of the HC-PCF (typical radius $\sim 5\ \mu$m). We ignore the initial condition of zero velocity, which should

[a)]laura.horan@tyndall.ie.
[b)]a.ruth@ucc.ie.
[c)]fatima.gunning@tyndall.ie.

produce negligible error due to the length of fiber used here. The model also assumes laminar flow and that the contact angle with the capillary walls remains constant throughout the filling process. This is a reasonable assumption, given the environmental conditions are stable and only Newtonian liquids are considered. Thus, the average flow velocity (v) will depend on the liquid's surface tension (σ) and viscosity (μ) and on the capillary radius ($r \sim 5\ \mu$m),

$$v = \left(\frac{r}{2L}\right)\left(\frac{\sigma}{\mu}\right) = \frac{L}{t}, \tag{1}$$

and is simply given by the ratio of fiber length (L ranging from 10–12 cm) to filling time (t). This relationship is unique to each liquid.[18] When the liquid's surface tension, the fiber length, and capillary radius are known, and the filling time is measured, the viscosity can be determined using Eq. (1).

In order to determine the surface tension of a solution with a given solute concentration of C, a well-known linear approximation utilizing static parameters may be used:[19]

$$\sigma = \left(\sigma_w + \frac{\Delta\sigma}{\Delta C} C\right)\cos\theta, \tag{2}$$

where σ_w is the surface tension of the solvent (PBS in our case), with a constant $\Delta\sigma/\Delta C = 1.3 \times 10^{-3}$ (N m^{-1})/M[19] for both glucose and fructose, and cos θ is the angle that the meniscus makes with the capillary walls. To determine the surface tension σ, the system is calibrated with the solvent only ($C = 0$). This is done by measuring the average flow velocity of the solvent PBS, and calculating the surface tension σ in Eq. (1), using the viscosity value from the literature.[20] The value found for σ is then inserted into Eq. (2) to determine the cosine of the contact angle, taking $\sigma_w = 0.0695$ N/m from literature.[21] In this experiment, the angle θ was estimated to be $\sim 50°$, using our results and known values for PBS. The viscosities of the saccharide solutions outlined in Sec. II D were then determined with Eq. (1) using the surface tension from Eq. (2) and the measured average velocity of the fluid.

B. Experimental setup

The fiber chosen was HC-PCF-1060 (NKT Photonics A/S), with an original primary PBG at 1060 nm, a secondary PBG at 735 nm, and a hollow core radius of $\sim 5\ \mu$m. The fiber core had a volume of 9.4 nl for a length of 12 cm. The total cross-sectional radius of the microstructure was 25 μm. For all experiments in this paper, the fiber segments were cleaved and not subjected to chemical pre-treatment.

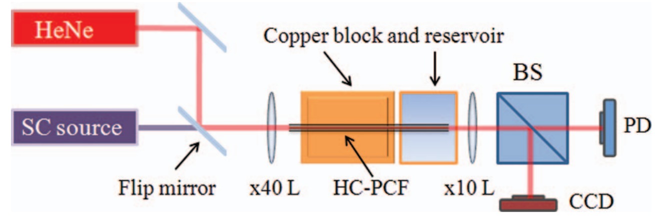

FIG. 1. Schematic of the viscometer experimental setup. A supercontinuum source (SC) was used to align the fiber with the aid of a $\times 40$ objective lens (L) to focus the light to the fiber. A flip mirror was used to guide 633 nm light during the fluid flow within the fiber. The output signal was collimated by a $\times 10$ objective lens, and divided by a beam splitter (BS) to enable light monitoring by a photodiode (PD) and a charged coupled detector (CCD).

The experimental setup used to determine the average velocity is schematically illustrated in Fig. 1. Two laser sources were used. The first was a supercontinuum source (SC) used for alignment of the empty fiber using a bandpass filter at 1050 nm (with 10 nm FWHM) and subsequently for characterizing the light propagation changes during fiber filling. This is discussed in more detail in Sec. II C below. The SC source consisted of a semiconductor-pumped Q-switched Nd:YAG laser at 1064 nm (6.85 kHz repetition rate, ~ 0.55 ns pulses, 73.5 mW average power), which pumped a highly nonlinear fiber (SC 5 1040, Blaze Photonics) and generated a broadband emission over the wavelength range (~ 400–1750 nm). The second source was a continuous wave (cw) HeNe laser (~ 1 mW, 633 nm) used in order to determine the average velocity of the liquid flowing through the fiber. In order to maintain the initial alignment, a flip-mirror was inserted in the setup to easily switch between optical sources. Light at 633 nm should initially experience high-loss because it falls outside the PBG of the empty fiber. However, once the fiber is filled with a liquid of refractive index ~ 1.33, the predicted PBG shift[9] would be centered at ~ 600 nm with a bandwidth of ~ 200 nm, enabling low-loss transmission of the HeNe laser light.

The collimated laser light was focused into the HC-PCF by a $\times 40$ objective lens. Fiber segments of 10–12 cm in length were chosen, which were long enough to enable accurate optical alignment, and yet short enough to limit the measurement time and to prevent excessive temperature variations. The fiber tips had their cladding jacket removed, 2 cm from each end, in order to allow cleaving of the ends for better light coupling.

Viscosity is strongly temperature dependent, and generally increases exponentially with decreasing temperature.[22] As such, steps were taken to ensure the fiber sample was kept at constant temperature along its length during the measurement. The schematic of our temperature control system is shown in Fig. 2. The *xyz* optical positioning stage (not shown in Fig. 2) holding the fiber was fitted with a 5-cm-long copper casing which kept the temperature of the fiber at 29.0 ± 0.1 °C with the aid of a thermoelectric Peltier cooler (TEC). The temperature was monitored by a thermistor positioned

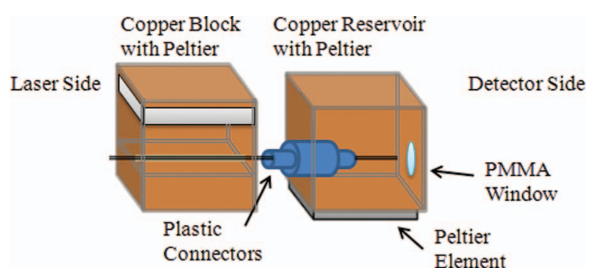

FIG. 2. Schematic for fiber holder and temperature control system for the HC-PCF (not to scale). Liquid is inserted into the reservoir on the right and the flow inside the fiber occurs from right to left of the figure. The laser light is launched at the left side of the figure, and detected by the PD and CCD at the right side via the PMMA window.

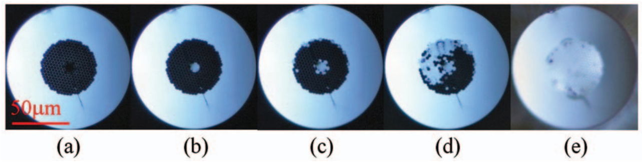

FIG. 3. Cross-sectional images of a HC-PCF-1060 showing its dynamic filling (a)–(e) observed via an optical microscope. The water reservoir, in this case, was placed at the other end of the fiber. The images show that the core fills faster (b) than the outer capillaries due to the difference in capillary radius.

just above the groove where the fiber was held in place. The fiber then exited the copper enclosure and entered the empty liquid reservoir through a series of plastic connectors in order to avoid leakage of the liquid when the reservoir is later filled. The reservoir had a small polymethyl methacrylate (PMMA) window on the detector side in order to allow the transmitted light to be collected. The reservoir was also maintained at a constant temperature, with an additional TEC and thermistor monitor placed at the side of the copper reservoir. Temperature could not be controlled within the plastic connectors, but this part of the fiber was kept to a minimum. These measures helped to minimize temperature gradients along the HC-PCF length.

To detect the propagation changes, the output of the fiber was collimated with a $\times 10$ infinity corrected lens (Fig. 1) to monitor the power of the light transmitted by the fiber. A beam splitter was added to facilitate initial alignment and near field monitoring with a charged coupled detector (CCD) camera (color sensor Sony ICX204AK). The signal from the low-speed photodiode (PD) (Silicon, active area 13 mm^2, 350–1100 nm, cathode grounded) was recorded with an analog-to-digital converter connected to a computer. The CCD images were recorded via USB at 30 frames/s.

C. Viscosity results

An optical microscope (Nikon Eclipse ME600) was used to understand the filling process in real time, as shown in Fig. 3. The HC-PCF-1060 was filled by water at one end and observed by an optical microscope with a magnification of $\times 50$ at the other. The images initially show the empty fiber (Fig. 3(a)), the point in time where only the core is filled (Fig. 3(b)), a sequence of gradual filling of the capillaries (Figs. 3(c) and 3(d)), and finally when the entire fiber is fully filled (Fig. 3(e)). The core fills faster than the capillaries due to its larger diameter, as expected by Eq. (1).

As a consequence, the light propagation during the filling process will also dynamically change, and different ranges of wavelengths will propagate at the different stages exemplified in Fig. 3. To illustrate the wavelength dependent propagation features, a selection of near-field color-sensitive CCD images was taken during the filling process and shown in Fig. 4 for a fiber sample of 10 cm. For that purpose, the broadband emission from the SC source was used to measure the light transmission during the filling. Initially ($t = 0$ s), only light at wavelengths within the original primary PBG centered around 1060 nm and secondary PBG are guided, as the reservoir is empty (Fig. 4(b)). Note that near-infrared wavelengths are detected by the CCD and are shown in Fig. 4(b) as an intense violet color. With increasing time, the filling fiber displays several guidance mechanisms. First, guidance by PBG effect dominates initially as the fiber is empty, and then changes to index guiding (once the core is fully filled), and finally to wavelength-shifted PBG (when all capillaries are filled). In more detail, while the fiber is initially filling, the HC-PCF segment at the laser side of the fiber is still empty, therefore the original PBG dominates and light at wavelengths outside the PBG bandgap are scattered. On the detector side of the fiber, however, where the fluid is filling the capillaries, some of the scattered light is able to couple back into the core either by index-like guiding or by the PBG shift (Fig. 4(c)). Eventually, after 114 s (Fig. 4(d)), the core is completely filled, the image from the CCD is saturated as an index-like guiding mechanism allows for a broad range of visible wavelengths to be propagated. After 340 s (not shown in Fig. 4), all capillaries are filled, and a PBG shift was observed. Evidence of this is shown in Figs. 4(e) and 4(f), when bandpass filters (FWHM 10 nm) centered at

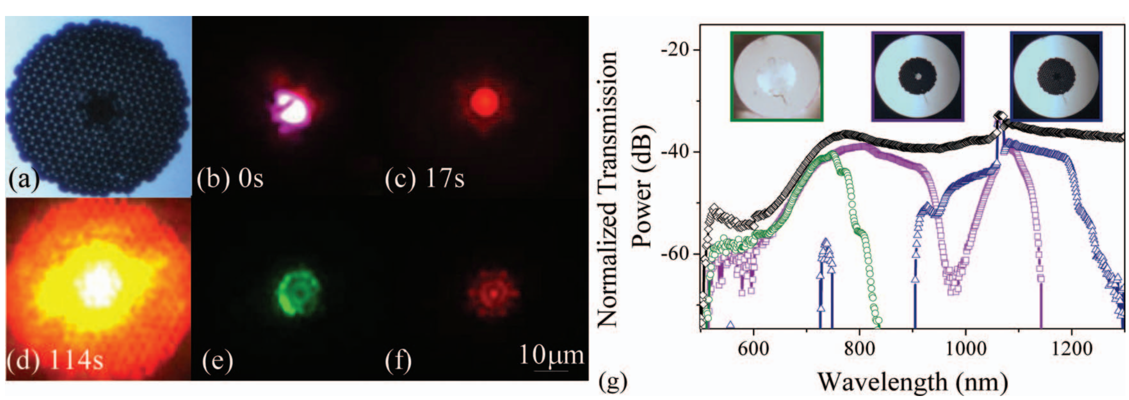

FIG. 4. (a) Image of the cross section of the HC-PCF-1060 fiber segment used taken by a Nikon Eclipse ME600 optical microscope. (b)–(d). Near-field images of the fiber transmitting broadband light from a supercontinuum source at different stages during the filling process. (d) Image of the fiber at 114 s when the core is filled. Panels (e) and (f) show pictures of the fiber where the light is transmitted through bandpass filters centered at 550 nm and 650 nm, respectively. Note: The CCD camera is light sensitive between 400 nm and 1100 nm. (g) Transmission spectra of 10 cm fiber segment when empty (blue triangles), core-only filled (purple squares), and fully filled (green circles). Also shown is the emission spectrum of the supercontinuum waveband (black diamonds.) Insets are the corresponding images depicting the filling states of the fiber in conjunction with the spectral outputs of the fiber for each filling state.

550 nm and 650 nm, respectively, were inserted to confirm the broad range of wavelengths guided between ∼500 and 800 nm.

The output spectrum of the HC-PCF was measured using an optical spectrum analyser (OSA), when the SC source was launched to the fiber, as in Fig. 1. The results are presented in Fig. 4(g), exemplifying the changes in guidance properties for the three different filling configurations: empty, core-only filled, and fully filled. The blue spectrum (triangles) shows guidance by the original PBG (Fig. 4(b)), with a maximum at 1060 nm, and a secondary band at ∼735 nm. The purple spectrum (squares) was recorded when only the core was filled, and where index guiding is the dominant guiding mechanism (Fig. 4(d)). This transmission exhibits two distinct peaks: the first, at 1060 nm, relates to the original PBG determined by the cladding capillaries structure, and a broadband guidance centered at ∼810 nm, due to index guiding effect. This broadband guidance had 3 dB (equivalent to a full width half maximum) and 20 dB bandwidths of at least 150 nm and 440 nm, respectively, and the spectrum is clipped at lower wavelengths due to the non-optimal condition of the supercontinuum source used at the time, as observed in the black spectrum (diamonds). The spectrum represented by green circles was measured when the entire fiber was filled with water. The spectrum features a shifted PBG at ∼750 nm (Figs. 4(e) and 4(f)), with a 3 dB bandwidth of at least 100 nm and a 20 dB bandwidth of 280 nm, respectively. The response of our SC source at lower wavelengths needs to be taken into consideration when analysing the PBG shift for the fully filled fiber.

The observations from Fig. 4 tell us that, with careful selection of the hollow core fiber and light sources, optical propagation can be either suppressed or supported depending on the filling state. Based on this principle, it is reasonable to expect that the use of a narrow-band source (in our case, a HeNe laser at 633 nm) will allow monitoring of the filling evolution of the core and the capillaries of a HC-1060 fiber, and hence determine the viscosity properties of the respective sample fluid.

Figure 5 shows the results obtained using the experimental setup from Fig. 1. After fiber alignment with the SC source, light coupling optimization with the HeNe laser source, and temperature stabilisation, the aqueous solution was inserted into the reservoir. Figure 5 shows the fiber transmission as a function of time, detected by the PD. Although no-guidance at the core was expected for the empty fiber at $t = 0$, a signal was still observed. We believe this is due to a small amount of scattered light from the core becoming confined in the solid cladding. Inserting the aqueous solution into the reservoir caused a sudden drop in the PD signal at ∼10 s. The initially decreasing PD signal in Fig. 5 was caused by changes in the output alignment of the fiber to the PD, due to refraction of the exiting beam when the liquid was inserted into the reservoir. However, this sudden drop also defined the start time t_0 for the filling process, and from here onwards the coupling remained constant. As the capillaries begin to fill, the change in the propagation properties is apparent. A rapid increase in transmission was observed just before $t \sim 200$s, which we believe coincides with the onset of index-guided propagation resulting from the filling of the fiber core. Once the core was fully filled after $t \sim 185$ s, the transmission remained almost constant.

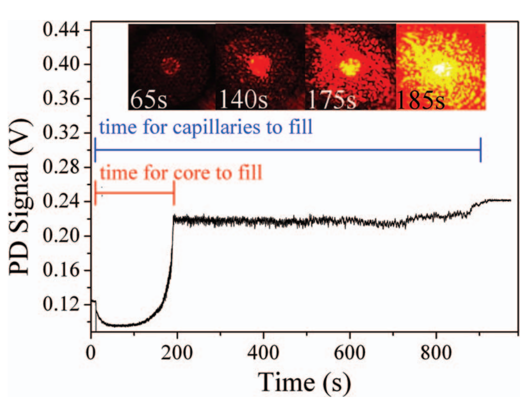

FIG. 5. HC-1060 fiber transmission at 633 nm as a function of time during the filling process. The fiber was filled with a 0.5 M solution of glucose in water in this example. The transmission is represented by the signal of the PD in units of volts. Insets show the near-field images of the output of the HC-PCF, captured by the CCD camera at different times.

A measurement of the core filling time is sufficient to determine the average velocity for the viscosity analysis as described in Sec. II A. Nevertheless, as the filling continued through the cladding capillaries, modal competition within the core was observed until the capillaries were completely filled after 900 s. The insets in Fig. 5 show the propagation changes captured by the CCD camera at different times during the filling.

D. Analyses for glucose and fructose solutions in PBS

To demonstrate the principles of operation of the proposed viscometer, phosphate buffer saline (PBS, purchased in tablet form from Sigma-Aldrich) was prepared by dissolving one PBS tablet in 200 ml of purified water to obtain 137 mM NaCl, 2.7 mM KCl, and 10 mM phosphate buffer solution. Solutions of D-(+)-glucose, ≥99.5% in PBS and D-(−)-fructose, ≥99% (Sigma-Aldrich) in PBS were prepared at concentrations ranging from 10^{-4} M to 1 M.

The average filling velocity ($\langle v \rangle$) was measured for these solutions as a function of concentration.[23] In Fig. 6(a), red diamonds (closed symbol) and blue squares (open symbol) represent the results for glucose and fructose solutions, respectively. For concentrations below 0.01 M, $\langle v \rangle$ appears to be constant with an average value of (1.1 ± 0.2) mm s^{-1}. The error was estimated from the uncertainty in measuring length and filling times of the fiber. The random variations of $\langle v \rangle$ for concentrations below 0.01 M are probably due to temperature fluctuations between measurements or temperature gradients within the setup. Above this concentration level, surface tension[19] and viscosity values increase. There is a notable decrease in the average velocity due to the decrease in the ratio of surface tension to viscosity. The experimental data in Fig. 6(a) were plotted and compared with a concentration dependant model based on Eq. (2) and a well-known relationship between viscosity and concentration from

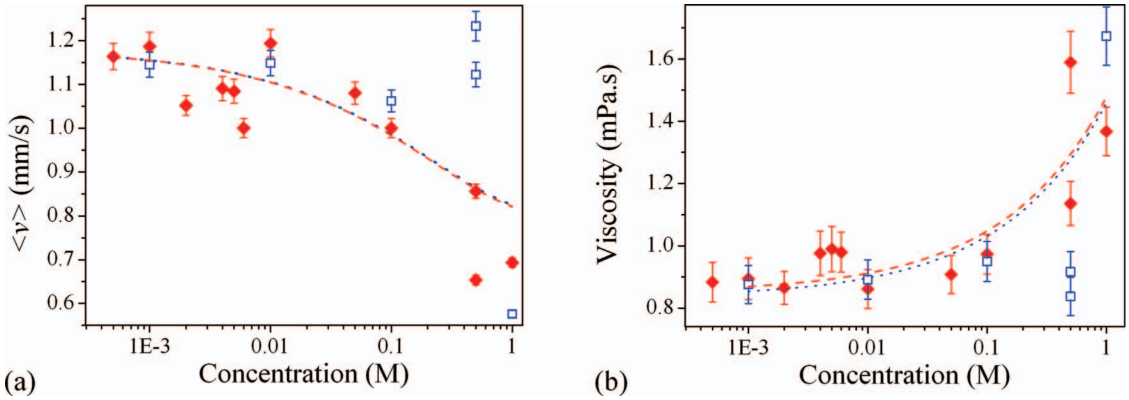

FIG. 6. Results obtained with the proposed viscometer. (a) Experimental average velocities for PBS solutions of glucose (red, closed diamond symbols) and fructose (blue, open squash symbols) for different concentrations at 29 °C. Red dashed line and blue dotted line are a ratio of Eq. (2) to Eq. (3), determined from literature.[20,23,27–29] (b) Measured viscosity from $\langle v \rangle$ with concentration for the glucose (red, closed diamond symbols) and fructose (blue, open squash symbols) in PBS solutions. The red dashed and blue dotted lines are fitted using Eq. (3) and data from the literature,[20,27–29] also presented in Table I.

Jones *et al.*[24]

$$\mu(C) = \mu_w + A\sqrt{C}, \quad (3)$$

where μ_w is the viscosity of the solvent and A is a parameter that depends on the solute. The value for μ_w is taken from literature to be 1.002 mPa s[20] and A is calculated from literature[20,26–29] by fitting Eq. (3) to the values outlined in Table I. For glucose, $A = 6.08 \times 10^{-4}$ (Pa s)/(M$^{1/2}$) and for fructose, $A = 6.01 \times 10^{-4}$ (Pa s)/(M$^{1/2}$). The ratio of Eq. (2) to Eq. (3) ($\sigma(C)/\mu(C)$) times a constant (r/2L) is then compared to the data acquired for the velocity of liquid flow in Fig. 6(a) for glucose (dashed red line) and fructose (dotted blue line) solutions.

The results for glucose and fructose are very similar,[25,26] as expected due to their similar physical parameters.

TABLE I. Viscosity values from literature for saccharide solutions in water.

Concentration (M)	Viscosity glucose (mPa s)	Viscosity fructose (mPa s)	Reference
0.028	1.01	1.01	Mathpal *et al.*[27]
0.056	1.02	1.02	
0.084	1.03	1.04	
0.112	1.05	1.05	
0.14	1.06	1.06	
0.168	1.08	1.08	
0.196	1.09	1.09	
0.224	1.11	1.10	
0.252	1.12	1.12	
0.28	1.14	1.13	
0.308	1.16	1.14	
0.336	1.17	1.16	
0	1.002		Comesaña *et al.*[20]
0.5	1.26		
1	1.59		
1.5	1.99		
0.27	1.36	1.26	Migliori *et al.*[28]
0.56	1.58	1.43	
1	2.13	2.09	
0.56	1.07	1.02	Telis *et al.*[29]
1	1.68	1.59	

The concentration-dependent viscosity was determined with Eq. (1), using surface tension values from Auman *et al.*[19] and Eq. (2) as described in Sec. II A. The results are shown in Fig. 6(b), in comparison with a selection of data from the literature,[20,27–29] which are represented by open symbols and outlined explicitly in Table I. The viscosity measurements from the literature were determined at similar temperatures in aqueous solutions, but different experimental approaches were utilized. Looking at the trends in Fig. 6(b), for low concentrations the changes in viscosity are expected to be within the error limit, as the amount of saccharide added to the solvent is very small. For higher concentrations, however, the viscosity becomes sensitive to the solute concentration. Figure 6(b) illustrates this dependence of the viscosity with increasing saccharide concentrations above 0.1 M, showing that the technique proposed here gives similar results than other well established techniques, with the advantages of small volumes being handled.

Although only saccharide solutions were used as test cases, it is evident that this is an effective technique for analyzing the viscosity of liquids in a simple optical setup, which could be miniaturized for a wide range of applications.

III. RAMAN SPECTROSCOPY USING HC-PCF

Small modifications to our setup can be implemented to allow Raman scattering measurements to be taken in real time as the HC-PCF fills, or after the filling process when the fluid is stable within all capillaries. The detection of Raman scatter from a sample mixture is a powerful analytical tool to identify individual molecular species within a sample. It is known that HC-PCFs can be used to increase the light-sample interaction path length and at the same time improve the light collection efficiency of Raman scattering.[15,30] Here we show that the Raman scattering can be incorporated with the viscometer technique, enabling dynamic analysis of the fluid while filling the capillaries. From our results, we identify that the optimum time to take a Raman signal is when the core of the fiber alone is filled with the liquid sample. During the subsequent filling of the capillaries in the micro structured cladding, the

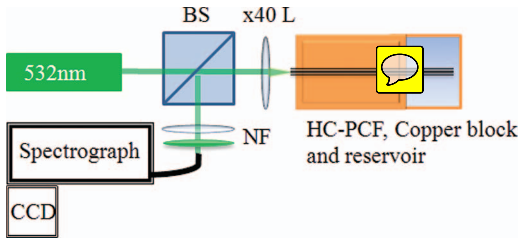

FIG. 7. Experimental setup for backscattered Raman experiments, after alignment as outlined in Sec. II B. Laser light from a frequency doubled cw Nd:YAG laser was launched to the HC-PCF via a beam splitter (BS) and a ×40 lens (L). While the transmitted signal was monitored via a CCD camera and a PD, as in Fig. 1, the backscattering was collected via a lens, a notch filter (NF) to block the excitation beam, and cooled Andor spectrometer.

inelastic scattering signal decreases by typically 40%-60% when the entire fiber is filled.

A. Experimental setup

A frequency doubled continuous wave (cw) Nd:YAG laser (∼10 mW at 532 nm) was used to optically pump the sample. The Raman scatter was detected with a backscatter configuration, as shown in Fig. 7. Raman backscatter was collected using a ×40 infinity correction lens, which was also used to focus the light into the fiber initially. The backscattered light passed through a beam splitter and a notch filter centered at 532 ± 17 nm (suppression 10^{-6}) to block light at the excitation wavelength. The inelastic (Raman) backscatter was focused onto a light guide with a lens. The light guide (fiber bundle with round entrance aperture and "slit" exit aperture) was connected to a polychromator with back-illuminated and cooled CCD detector (Andor DV401, −30 °C) with a resolution of 0.2 nm. The output of the fiber in the forward scattering regime is continuously monitored by a CCD camera and PD, as detailed in Sec. II B, and shown in Fig. 1 (detector side).

Precise control of the light guidance was crucial, and the positioning of the lenses, beam splitter, and the HC-PCF segment in the setup was adjusted to maximize the collection of the Raman signal. Backscattered Raman signal from the silica cladding can decrease the sensitivity of our measurement, and slight optical misalignments will lead to a significant decrease of the signal-to-noise ratio.

B. Raman spectra of saccharide solutions

The setup was used to identify the well-known spectra for solutions of glucose and fructose diluted in PBS inside a fully filled HC-PCF, shown in red and blue in Fig. 8, respectively, and for the wavenumber range between 290 and 3900 cm^{-1} with an integration time 60 s. To obtain the spectra in Fig. 8, a background spectrum for a fiber filled with solvent PBS only was subtracted, accounting for any scattering from the fiber itself and PBS. The light guiding properties of the fiber may cause the resulting Raman scatter intensities to differ slightly to those acquired from a bulk sample. However, the spectral region addressed comprises the characteristic C–O and C–C stretch vibrations at 900, 1100, and 1350 cm^{-1} for glucose and 600, 1230, and 1430 cm^{-1} for fructose, allowing the identification of the two monosaccharides.[31]

C. Simultaneous viscometer and Raman analysis

To demonstrate the feasibility of integrating the viscometer with the Raman scattering setup, a kinetic series of Raman spectra was collected during the filling of a 12 cm HC-PCF with 1 M glucose solution. The same experimental procedure described in Sec. II B was applied, by exchanging the HeNe laser (centered at 633 nm) with a cw frequency-doubled Nd:YAG laser at 532 nm. A series of 800 Raman backscatter measurements was taken, as the fiber was filled, each measurement having an integration time of 1s, with the wavenumber shift measured sequentially over a range of 4000 cm^{-1}, and a selection of results is plotted in Fig. 9(a). Initially no backscattering was observed until 350 s. This time corresponds to the core of the fiber being filled by ∼90%. The signal strength reached a maximum at ∼360 s, when the core was fully filled, enabling propagation of broadband light, but it decayed again after that.

In order to understand the dynamics of the Raman scattering signal strength, one must look closely to the optical propagation properties, as discussed in Sec. II C. Along with the backscattering, the optical power through the fiber was

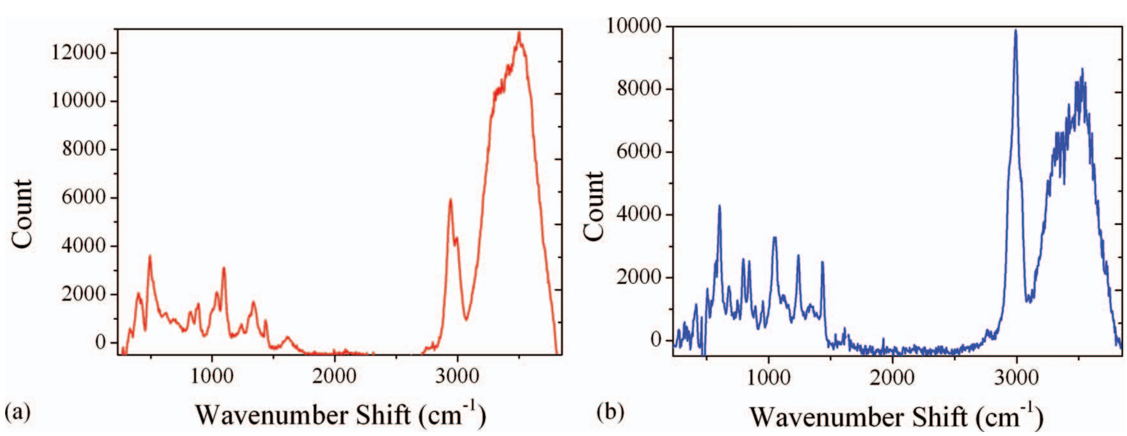

FIG. 8. Stokes Raman spectra for 1M (a) glucose (red) and (b) fructose (blue) in PBS solutions contained within a HC-PCF. Integration times for samples in the HC-PCF was 60 s.[31]

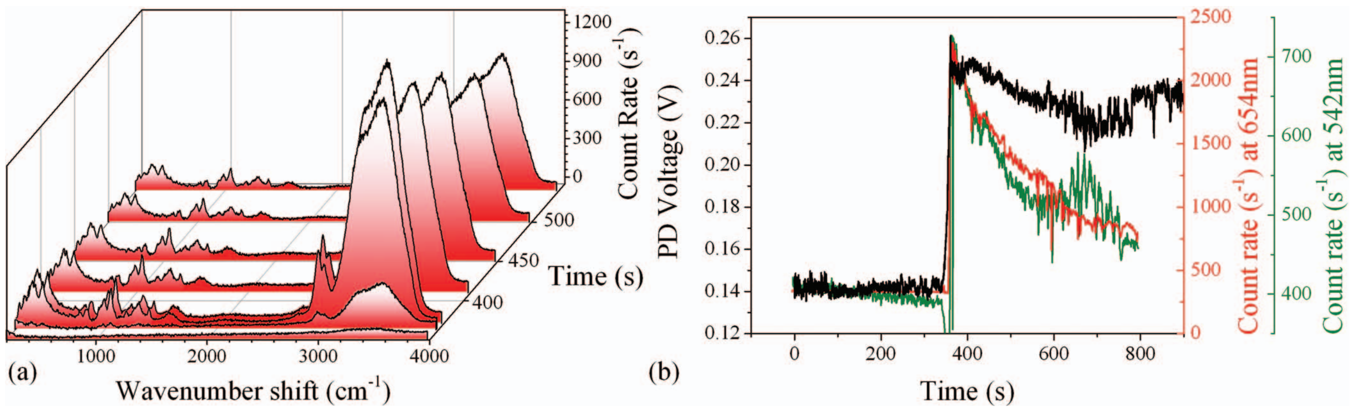

FIG. 9. Results for an integrated viscometer and Raman scattering system using a 12 cm HC-PCF for a 1 M glucose solution in PBS. (a) Dynamic Raman backscatter taken every 1 s (integration time). (b) Transmission results for photodiode signal (black) during filling, normalised Raman signal at 3500 cm^{-1} (red 654 nm) and 350 cm^{-1} (green 542 nm) as a function of time.

also monitored with the assistance of a photodetector (shown as PD in Fig. 1). This signal, for the 532 nm pump, is plotted in Fig. 9(b) (black) showing that, at ∼360 s, a sharp increase in power is observed due to the core being completely filled. This is in agreement with the investigations in Sec. II C, where we show that if the core only is filled with a fluid, visible and near infra-red light is allowed to propagate by index guiding effect. Although it is not clear from Fig. 4(g) if 532 nm light is allowed to propagate, experimentally we observed that it can, even though the power levels may be smaller (Fig. 9(b), black). This is also true while the cladding capillaries were being filled ($t > 360$ s).

The 532 nm signal shows a 20 s rise time, corresponding to the change from almost no guidance to full guidance in the fiber core at 360 s. The 633 nm signal shows a much longer rise time of ∼70 s (see data in Fig. 5), and hence the filling time of the core can be determined more accurately using a 532 nm pump as this wavelength does not fall within the initial PBG of the fiber. It should be noted that the data in Fig. 5 is for a 0.5 M solution of glucose with an expected viscosity of 1.26 mPa s, and the data in Fig. 9(b) is for a 1 M glucose solution with an expected viscosity of 1.58 mPa s, which results in a longer filling time than shown in Fig. 5. This implies that using a different laser source may enhance the accuracy of the time measurements of the viscometer. The red trace in Fig. 9(b) shows the evolution of the Raman signal at 3500 cm^{-1} (corresponding wavelength ∼654 nm). In this case, no signal is observed before 350 s, just like the PD signal, after which a sharp increase in the count rate was measured, again due to the core being fully filled.

Once the core is filled and the capillaries continue to fill, the count rate of the inelastically scattered light starts to decrease as the guiding mechanism changes slowly from index-guiding to a shifted PBG (red trace in Fig. 9(b)). To determine if the time dependence of the signal is similar over the entire spectral range concerned, the intensity at a shift of at 350 cm^{-1} (corresponding wavelength ∼542 nm) is plotted in green in Fig. 9(b). A lower count rate is observed, but the decay in signal is similar to that at 654 nm. One of the reasons for this decay may be that the modal distribution changes when shifting from strong index-guiding, for the core-only filled case, to weakly guidance once fully filled, reducing the power density of the signal, and hence reducing the backscattered signal.

Nevertheless, from the results, it is clear that an optimum Raman scatter can be obtained from a fiber when only the core is filled, and when the source is carefully selected to maximize the signal.

IV. CONCLUSIONS

We successfully utilized a novel technique to determine when the core and capillaries of a HC-PCF are filled with liquid, and thus determine the average velocity of the liquid, and hence its viscosity. The HC-PCF is identified as an ideal vessel for the viscosity measurement of nanoliter quantities of sample, especially important for applications in pharmaceutical and biosciences areas. We analysed the technique for glucose and fructose solutions in PBS, and demonstrated good agreement with values previously published in the literature. Our viscometer has the additional advantage of being easily integrated to a Raman scattering systems, allowing simultaneous analysis of viscosity and Raman spectral information.

ACKNOWLEDGMENTS

The authors would like to acknowledge Jiadi Lu, Monika Rutowska, and Andrew Ellis for their support and useful discussions. This project is funded by an IRCSET grant, SFI grant 6/IN/I969 and 11/RFP.1/PHY/3233.

[1]T. A. Birks, P. J. Roberts, P. S. J. Russell, D. M. Atkin, and T. J. Shepherd, Electron. Lett. **31**(22), 1941–1943 (1995).
[2]P. Russell, Science **299**(5605), 358–362 (2003).
[3]R. F. Cregan, B. J. Mangan, J. C. Knight, T. A. Birks, P. S. J. Russell, P. J. Roberts, and D. C. Allan, Science **285**(5433), 1537–1539 (1999).
[4]J. B. Jensen, L. H. Pedersen, P. E. Hoiby, L. B. Nielsen, T. P. Hansen, J. R. Folkenberg, J. Riishede, D. Noordegraaf, K. Nielsen, A. Carlsen, and A. Bjarklev, Opt. Lett. **29**(17), 1974–1976 (2004).
[5]M. S. Rutowska, F. C. G. Gunning, F. Kivlehan, E. Moore, D. Brennan, P. Galvin, and A. D. Ellis, Meas. Sci. Technol. **21**(9), 094016 (2010).
[6]S. Smolka, M. Barth, and O. Benson, Appl. Phys. Lett. **90**(11), 111101 (2007).
[7]J. C. Knight and P. S. J. Russell, Science **296**(5566), 276–277 (2002).

[8]T. Birks, D. Bird, T. Hedley, J. Pottage, and P. Russell, Opt. Express **12**(1), 69–74 (2004).
[9]G. Antonopoulos, F. Benabid, T. A. Birks, D. M. Bird, J. C. Knight, and P. S. J. Russell, Opt. Express **14**(7), 3000–3006 (2006).
[10]J. M. Fini, Measurement Sci. Technol. **15**(6), 1120 (2004).
[11]E. C. Bingham, J. Ind. Eng. Chem. (Seoul, Repub. Korea) **6**(3), 233–237 (1914).
[12]H. Cotton, P. A. Rebers, E. Maudru J, and G. Rorabaugh, *Use of Sugars and Other Carbohydrates in The Food Industry* (American Chemical Society, 1955), Vol. 12, pp. 3–20. Q1
[13]P. Arabie and H. Moskowitz, Atten. Percept. Psychophys. **9**(5), 410–412 (1971).
[14]Y. Komachi, H. Sato, Y. Matsuura, M. Miyagi, and H. Tashiro, Opt. Lett. **30**(21), 2942–2944 (2005).
[15]A. Khetani, V. S. Tiwari, A. Harb, and H. Anis, Opt. Express **19**(16), 15244–15254 (2011).
[16]K. Nielsen, N. Danny, S. Thorkild, B. Anders, and P. H. Theis, J. Opt. A, Pure Appl. Opt. **7**(8), L13 (2005).
[17]E. W. Washburn, Phys. Rev. **17**(3), 273–283 (1921).
[18]A. H. Pelofsky, J. Chem. Eng. Data **11**(3), 394–397 (1966).
[19]E. Aumann, L. M. Hildemann, and A. Tabazadeh, Atmos. Environ. **44**(3), 329–337 (2010).
[20]J. F. Comesaña, J. J. Otero, E. García, and A. Correa, J. Chem. Eng. Data **48**(2), 362–366 (2003).
[21]A. T. Palasz, J. Thundathil, R. E. Verrall, and R. J. Mapletoft, Anim. Reprod. Sci. **58**(3–4), 229–24015 (2000).
[22]A. A. Ruth, H. Lesche, and B. Nickel, Z. Phys. Chem. **217**(6-2003), 707–722 (2003).
[23]E. Horan, G. Khara, M. Rutowska, A. D. Ellis, and F. C. G. Gunning, paper presented at the OFS21, Ottawa, Canada, 2011.
[24]G. Jones and S. K. Talley, J. Am. Chem. Soc. **55**(2), 624–642 (1933).
[25]J. Chirife and M. P. Buera, J. Food Eng. **33**(3–4), 221–226 (1958).
[26]T. Soesanto and M. C. Williams, J. Phys. Chem. **85**(22), 3338–3341 (1981).
[27]R. Mathpal, B. K. Joshi, S. Joshi, and N. D. Kandpal, Monatsch. Chem. **137**(3), 375–379 (2006).
[28]M. Migliori, D. Gabriele, R. Di Sanzo, B. de Cindio, and S. Correra, J. Chem. Eng. Data **52**(4), 1347–1353 (2007).
[29]V. R. N. Telis, J. Telis-Romero, H. B. Mazzotti, and A. L. Gabas, Int. J. Food Prop. **10**(1), 185–195 (2007).
[30]X. Yang, A. Zhang, D. Wheeler, T. Bond, C. Gu, and Y. Li, Anal. Bioanal. Chem. **402**(2), 687–691 (2012).
[31]S. Söderholm, Y. H. Roos, N. Meinander, and M. Hotokka, J. Raman Spectrosc. **30**(11), 1009–1018 (1999).